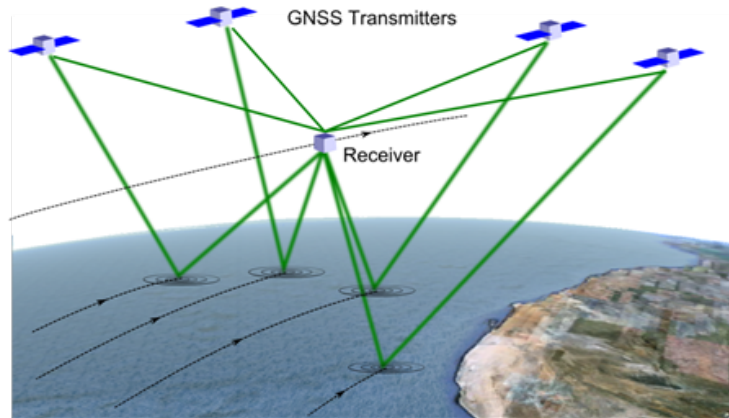


Sea Surface Altimetry using GNSS-R



Bachelorarbeit im Studiengang
Geodäsie und Geoinformatik
an der Universität Stuttgart

Fanxiang Li

Stuttgart, July 2018

Betreuer: Prof. Dr.-Ing. Nico Sneeuw
Universität Stuttgart

Erklärung der Urheberschaft

Ich erkläre hiermit an Eides statt, dass ich die vorliegende Arbeit ohne Hilfe Dritter und ohne Benutzung anderer als der angegebenen Hilfsmittel angefertigt habe; die aus fremden Quellen direkt oder indirekt Übernommenen Gedanken sind als solche kenntlich gemacht. Die Arbeit wurde bisher in gleicher oder ähnlicher Form in keiner anderen Prüfungsbehörde vorgelegt und auch noch nicht veröffentlicht.

Ort, Datum

Unterschrift

Abstract

The Global Navigation Satellite Systems Reflectometry (GNSS-R) aims to retrieve information about the Earth surface by analyzing the signals emitted by GNSS transmitters (such as GPS, GLONASS, GALILEO and COMPASS...), and captured by an elevated platform after the signal has rebounded off of the oceans, lakes, land or ice and snow. The sea surface altimetry is an essential oceanic application of the GNSS-R. In this thesis, a method is introduced to solve this altimetric problem. Besides, a set of experimental data based on the campaign "Gold Test" carried out over the Mediterranean sea in 2005 provided by Institut de Ciències de l'Espai (ICE) is tested.

Contents

1	Introduction	1
1.1	GNSS and GNSS-R	1
1.2	GNSS-R Altimetry	2
1.3	Comparison with Conventional Altimetry	3
1.4	Applications	4
1.5	Outline of this Thesis	4
2	Methodology	5
2.1	Geometry of the GNSS Reflection and Conventions used in this Thesis	5
2.2	The General Form of the Altimetric Equation	8
2.2.1	Geometric Delay ρ_{geo}	8
2.2.2	Atmospheric Delay ρ_{atm}	9
2.2.3	Instrument Delay ρ_{ins}	9
2.2.3.1	Eccentricity Delay	10
2.3	Specular Point Height Estimation Method	11
2.3.1	Determine the Position of Transmitter and Receiver	11
2.3.2	The 2-D Position (Longitude and Latitude) on the Ellipsoid Surface	11
2.3.3	The 3-D Position (Longitude, Latitude and ell. Height) of the Specular Point	15
2.3.4	Summary	18
3	A Specific Example	19
3.1	Data Sources: GOLD_RTR Mining	19
3.2	Campaign "Gold Test"	20
3.2.1	Observations	21
3.2.2	The Ellipsoidal Height of the Specular Point	27
3.2.3	The Orthometric Height of the Specular Point	28
4	Conclusion and Outlook	33
4.1	Conclusion	33
4.2	Outlook	33

List of Figures

1.1	Geometry of a Radar Imaging System [3]	3
2.1	Geometry of a GNSS Reflection	5
2.2	Sketch of the GNSS-R as a Multi-Static System of Observation [6]	6
2.3	Delay between the Transmitter and the Receiver	8
2.4	Sketch of the Body Frame Coordinate System used to provide the Offset between Antennas [11]	9
2.5	Find the Specular Point for 2-D Circumstance	14
2.6	Geometry of the Receiver, Earth Ellipsoid, Sea Surface, direct and reflected Signal Paths	15
2.7	Flowchart of the SSH Calculation	16
2.8	Explanation of the Height Estimate Update	17
2.9	Summary of the Method	18
3.1	Overall Summary of each Campaign	19
3.2	Tracks of the reflected Signals captured in different Campaigns	20
3.3	The Aircraft and the Hardware applied during the Measurement	20
3.4	Satellites used during the Measurements	22
3.5	The Frequency Percentage of simultaneously visible GNSS Transmitters from a Receiver [11]	23
3.6	The Elevation Angle	23
3.7	The Eccentricity-, atmospheric- and geometric Delay	24
3.8	The Receiver Position	25
3.9	The Transmitter Position	26
3.10	The ell. Height of the Specular Point	27
3.11	The Undulation of the Geoid	28
3.12	The ort. Height of the Specular Point	29
3.13	The ort. Height of the Specular Point (for a small Area)	30

List of Tables

2.1	Abbreviations and Acronyms	7
2.2	Example of the Offset Vectors (First Flight on 13.07.05)	10
3.1	The Time at the Begin of the Measurement of each Flight	21

Chapter 1

Introduction

1.1 GNSS and GNSS-R

The Global Navigation Satellite System (GNSS) has become a very important and powerful contributor to all scientific questions related to precise positioning on Earth's surface since Global Positioning System (GPS) became fully operational in 1994, particularly as a mature technique in geodesy and geosciences. With the development of GNSS as a satellite microwave (L-band) technique, more and wider applications and new potentials are explored and utilized. The versatile and available GNSS signals can image the Earth's surface environments as a new, highly precise, continuous, all-weather and near-real-time remote sensing tool.

Generally, a multipath signal in positioning is often considered as an undesirable phenomenon that needs to be suppressed. A reflected GNSS signal is one kind of multipath, also known as a scattered signal. Usually, the reflected signal is regarded as one of the main error source that deteriorates the positioning accuracy. It has been recognized, however, these scattered signals can also be used in many remote sensing applications to sense the Earth's surface environments. A number of experiments and missions using GNSS reflected signals from ocean and land surface have been tested and applied.

Remote sensing based on processing and analyzing reflected GNSS signals is commonly termed GNSS reflectometry (GNSS-R). Investigating the use of reflected Global Navigation Satellite System (GNSS) signals for remotely sensing the Earth's surface, was first proposed in early 1990s by ESA [15] to provide additional measurements of the sea surface to increase the spatial and temporal resolution of the Radar Altimeters (RA), which typically only measure the ocean height at the sub-satellite point (mono-static, nadir-looking systems). The signal measurement precision level of the LEO-based GNSS-R is expected lower than standard space-based microwave RA. However, the potential temporal and spatial coverage/resolution of the concept suggests its complementarity with mono-static RA [11].

The GNSS signals are always available, globally, and the signal structures are typically well known, except for those dedicated to military use. Furthermore, the GNSS signals have some distinctive characteristics which can be utilized for remote sensing purposes. Recently there has been an increase in such investigations by academia and research institutions, partly because this innovative use of GNSS signals has many potential applications. In particular, space agencies such as NASA and ESA have already funded, or are going to fund, a number of projects/missions which focus on the applications of GNSS reflectometry [18]. An example is the ESA's Passive Reflectometry and Interferometry System (PARIS) project. PARIS can be used as a passive radar altimeter. Different from current radar altimeters, PARIS would measure

multiple samples from different tracks and rapidly form images of mid-sized (mesoscale) phenomena such as ocean currents or tsunamis [8]. However, there are still many challenging problems to be resolved, especially when applying this reflectometry technique to a range of application scenarios.

When building a GNSS-based remote sensing system, only the receiver needs to be designed and manufactured. The receiver platform (static or mobile; land-based, air-based, or satellite-based) needs to be selected based on the specific application.

In the case of an aircraft or satellite platform, the direct signal is received via a zenith-looking right-hand-circularly-polarized (RHCP) antenna, while the reflected signal is collected through a nadir-looking left-hand-circularly-polarized (LHCP) antenna. The reason for such an antenna selection is that GNSS signals are designed as RHCP; however, the reflected GPS signals have a distinct characteristic, that is when reflected over a ground surface, they are changed to be LHCP. In the case of a land-based platform, either two antennas are used to receive the direct and reflected signals separately or a single antenna is used to capture both the two signals. For some applications it is desirable that both direct and reflected signals interfere with each other, being then gathered by a single antenna pointing towards the horizon, the Earth limb, or at certain slant orientation [11].

There is a range of geophysical and geochemical parameters which can be measured using a GNSS-based reflectometry system, including soil moisture, salinity, sea surface height (SSH), sea surface wind speed and wind direction, snow and ice thickness and even biomass density. For example a number of researchers have investigated ocean surface altimetry using measurements obtained by either mounting the receiver on an aircraft, or fixing it on the ground such as on a bridge [17]. Besides, a limited number of signals have been detected in space using a very high gain antenna.

The Global Positioning System (GPS) coarse/acquisition (C/A) code (also termed clean code) or the GPS P(Y) code was employed to do the measurement. The P(Y) code can be used to achieve accuracy which can be higher than that when using the C/A code alone; however, the P(Y) code structure is not known to the civilian community.

1.2 GNSS-R Altimetry

The altimetric techniques can in principle be applied to reflections off any surface, but their performance will depend on the signal-to-noise ratio of the scattering. Therefore, GNSS-R altimetry has only been conducted on strongly reflecting surfaces and geometries, such as waters and smooth ice, or land at near-surface receiver altitudes.

In this thesis the focus is on GNSS-based ocean surface altimetry. The known C/A code is employed. The direct and reflected signals are received via two different antennas and then processed separately. The code phase of the direct signal and that of the reflected signal are estimated using a correlation delay waveform, and then used to estimate the delay of the reflected signal relative to the direct signal (this technique is not discussed in this thesis). The relative delay (i.e. the time difference of arrival between the reflected and direct signals) is then used to estimate the SSH.

1.3 Comparison with Conventional Altimetry

Conventional single radar remote sensing of the ocean requires dedicated transmitters and receivers with large directional antenna to achieve high resolution, while GPS as a bistatic radar system, requires only a receiver, not a transmitter, and can receive signals from global covering GPS satellites.

Although the satellite radar technique measures sea surface height at high spatial resolution along its ground track, the cross track distance is usually quite large (e.g., about the order of 300 km for TOPEX/Poseidon). Furthermore, the temporal resolution is lower with the 10-day repeat orbit of TOPEX/Poseidon, so it is too coarse for monitoring the sea surface. The GPS reflected signals from the ocean surface can measure the ocean surface height with high temporal-spatial resolution. Therefore, the new applications of GPS reflected signals from the ocean surface could compensate these defects of existing techniques, e.g., radar altimetry [12].

The figure below shows the geometry of a typical strip-mapping synthetic aperture radar imaging system. The antenna's footprint sweeps out a strip parallel to the direction of the satellite's ground track.

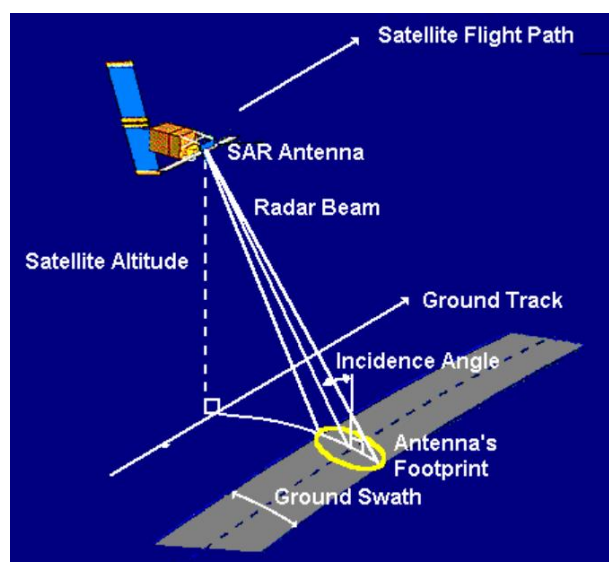


Figure 1.1: Geometry of a Radar Imaging System [3]

Therefore, the reflected GNSS signals can image the Earth's surface environments as a new, highly precise, continuous, all-weather and near-real-time remote sensing tool, which is expected to revolutionize various atmospheric sounding, ocean remote sensing and land/hydrology mapping, especially for various Earth's surfaces and atmosphere.

With the development of the multi-frequency and multi-system GNSS constellations, including Russia's restored GLONASS, the European Union's GALILEO system and China's Beidou/COMPASS system as well as a number of Space Based Augmentation Systems, such as Japan's Quasi-Zenith Satellite System (QZSS) and India's Regional Navigation Satellite Systems (IRNSS), more applications and opportunities will be exploited and realized using new onboard GNSS receivers on future space-borne GNSS reflectometry missions in the near future.

1.4 Applications

GNSS altimetry, with its higher spatial and temporal sampling, could make contributions to the following research topics [11]:

- **Eddies and Fronts** are essential to understand ocean circulation on all space and time scales, but a large fraction of their kinetic energy is associated with spatial scales that cannot be resolved with a single radar altimeter. Mesoscale variability is key to understand large-scale circulation and climate variability through eddy transport of momentum in interactions with the mean flow and meridional heat transport. GNSS altimetry, with its relatively large number of simultaneous measurements, can provide greater spatial and temporal resolution, and these can be traded against each other for a particular application.

- **Tsunamis** at open waters have a relatively small vertical signal (typically a few decimeters) but very large horizontal pattern, corresponding to ocean waves of long periods and long wavelengths. Its detection and warning must be as quick as possible, preferably 15 min after its origin. The synoptic-view capabilities of the GNSS-R system might help detecting them timely.

- **Geostrophic Velocities and Gravity Anomalies** are estimated based on measurements of the surface slope. Radar altimeters can measure surface slopes only in one direction - along track, except at widely time-spaced track crossover points. With GNSS altimetry, the slope measurements could be done along the path of the multiple simultaneous specular points on the surface. Over time, a single resolution cell would be crossed by several such paths, in different orientations. This potentially allows 2-D surface slopes to be estimated for larger set of resolution cells.

- **Tides**, in particular higher-order tidal components, might be better identified than in standard RA because of the non-repeating nature of the GNSS concept. Another possible advantage of the GNSS-R altimetry could be better sampling of internal tides, of wavelengths below about 100 km. These tides play an important role in large-scale circulation and vertical mixing in the deep ocean.

- **Physical-Chemical-Biological Intersections** mostly occur at scales not resolved with radar altimeters. One of the more important of these intersections is the oceans connection to the carbon cycle, which is crucial to understanding long-term climate variations.

1.5 Outline of this Thesis

In this thesis, an algorithm to calculate the 3-D position of the specular point in cartesian coordinate system as well as in geographic coordinate system with ellipsoidal height will be provided. Further more, if the information about the undulation of the study area is available, then the orthometric height is also calculable. This is the main task of this thesis and it is tackled in chapter 2. With the well designed algorithm a set of data (Campaign "Gold Test") provided by Institut de Ciències de l'Espai is tested in Chapter 3. This campaign took place over the Mediterranean Sea along the Catalanian north coast on 13 and 14.07.2005. All the required measurements are also demonstrated and explained in this chapter. The last chapter gives a conclusion on this thesis and an outlook on further development around this topic.

Chapter 2

Methodology

2.1 Geometry of the GNSS Reflection and Conventions used in this Thesis

The GNSS-R works as a bi-static radar: a system in which the transmitter and the receiver are separated by a significant distance, comparable to the expected distance to the target, as sketched in figure 2.1.

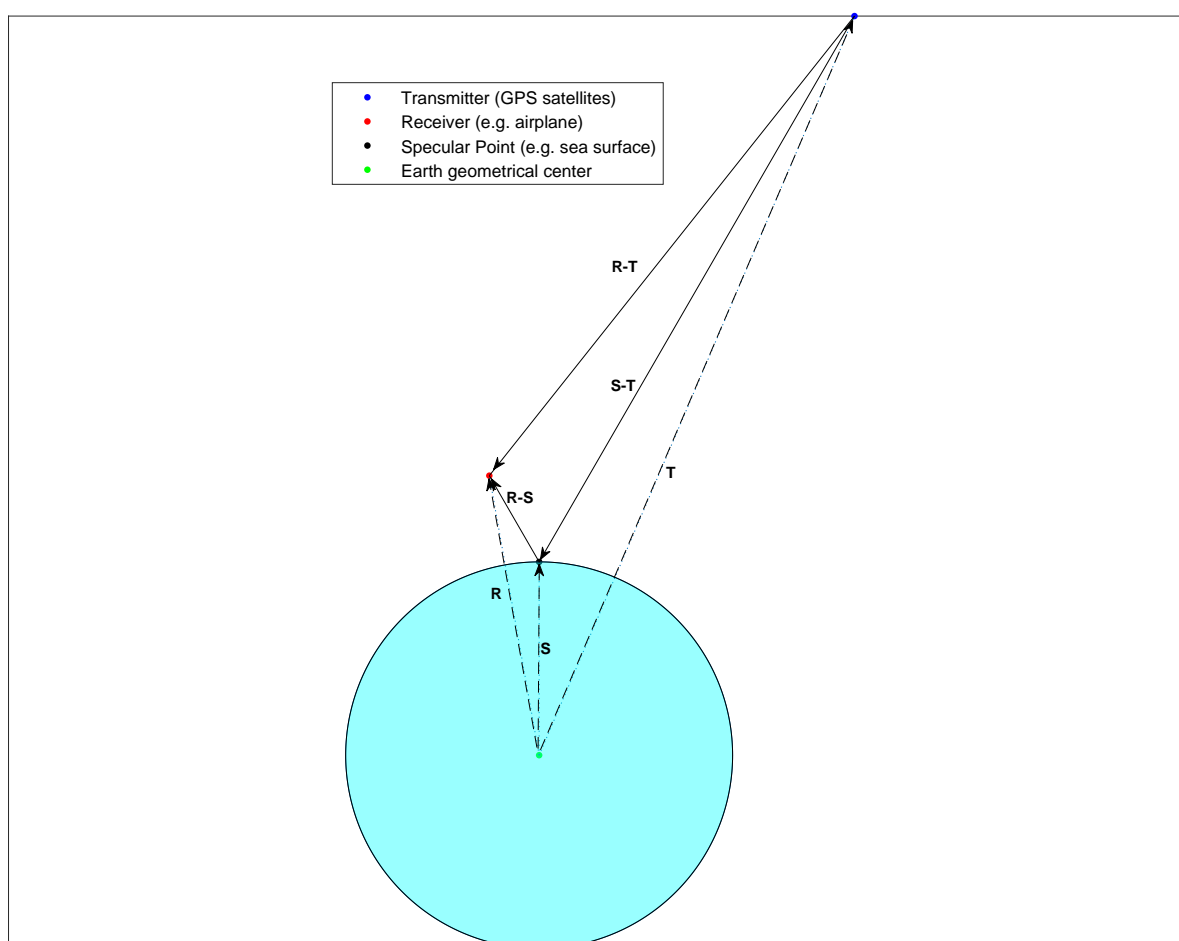


Figure 2.1: Geometry of a GNSS Reflection

This definition can be extended to a system in which a single receiver can simultaneously track a diversity of bi-statically reflected signals, from a diversity of different transmitting sources. Then we call it multi-static (see figure 2.2).

From each individual receiver, a large number of GNSS transmitted signals can be collected after their reflection off the Earth surface. This set of bi-static observations occur at different azimuth and elevation angles. As the receiver moves along its trajectory, the scanned surface takes an irregular and highly dense swath comb-like pattern.

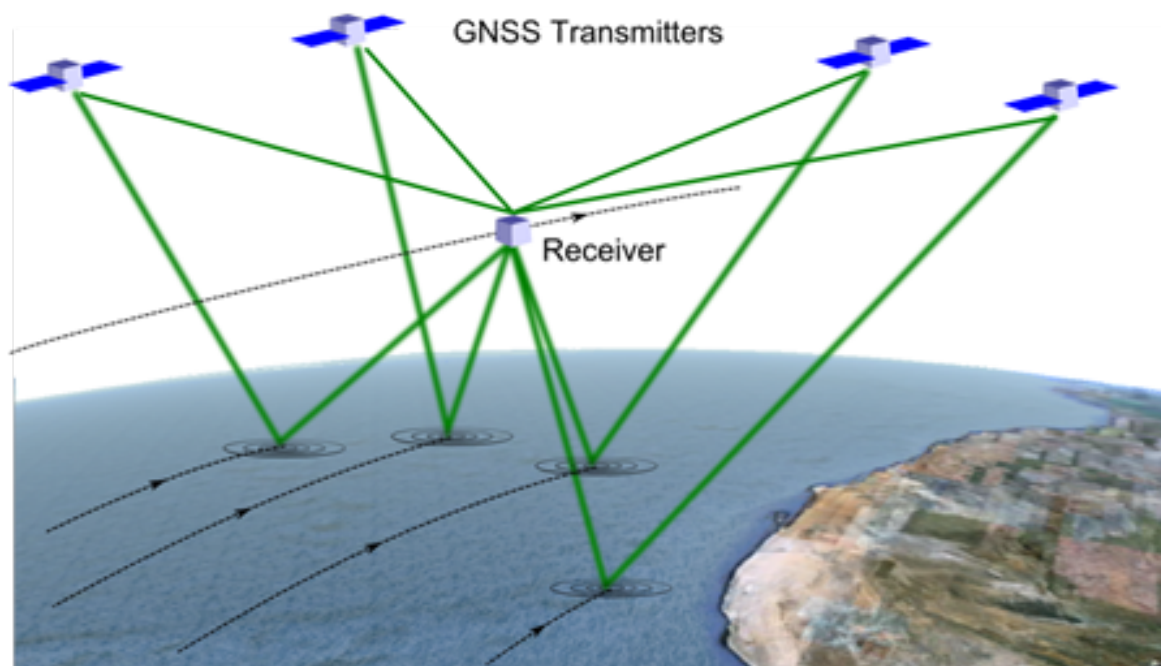


Figure 2.2: Sketch of the GNSS-R as a Multi-Static System of Observation [6]

The electromagnetic field at the receiver site has contribution from several GNSS sources (transmitting satellites), an important task it to distinguish them. Different GNSS transmitters can be identified and separated from the rest of transmitters being received simultaneously by the modulation applied to each GNSS. These contributions correspond to signals that have propagated directly from the source to the receiver, crossing the atmosphere; as well as signals that have propagated down to the Earth surface, reflected off its surface, and up to the receiver.

We will call "rays" or "radio-links" these different branches of the signal indistinctly. In principle, these two sort of contributions can be separated using two different antennas, one pointing to the transmitters to gather direct rays, and the other to the surface, to collect Earth-surface reflected signals. If the receiver is at air-borne or at higher altitudes, the delay and Doppler information can also be used to separate both radio-links [11].

Note that other contributions to the receiver electromagnetic field are also possible, such as those coming from atmospheric ducting (atmospheric multi-path), or from reflection off other objects surrounding the receiver or along the propagation path (such as aircraft wing and plates in airborne campaigns or tower pieces and other nearby equipment in ground-based experiments). These contributions will be neglected in this thesis.

Table 2.1 is a list of abbreviations and acronyms used throughout this thesis.

Abbreviations and Acronyms	Full Name
C/A code	Coarse Acquisition code
CSIC	Consejo Superior de Investigaciones Científicas
ECEF	Earth-Centered Earth-Fixed
ESA	European Space Agency
GNSS-R	Global Navigation Satellite Systems-Reflectometry
GPS	Global Positioning System
GLONASS	GLOBal NAVigation Satellite System
GOLD-RTR	GPS Open-Loop Differential Real-Time Receiver
ICE	Institut de Ciències de l'Espai
IEEC	Institut d'Estudis Espacials de Catalunya
L(R)HCP	Left(Right)-Hand-Circularly-Polarized
NASA	National Aeronautics and Space Administration
PARIS	PAssive Reflectometry and Interferometry
PRN	PseudoRandom Noise
RA	Radar Altimetry
SPP	Specular Point Position
SSH	Sea Surface Height
TPL	Total Path Length
UTC	Universal Time Coordinated
WGS84	World Geodetic System 1984

Table 2.1: Abbreviations and Acronyms

2.2 The General Form of the Altimetric Equation

The GNSS-R can measure the electromagnetic slant delay between the transmitter and the receiver, after the signal rebounds off the sea surface, ρ (see figure 2.3). This electromagnetic delay contains a geometric component ρ_{geo} due to the total geometrical distance travelled by the signal; it also includes atmospheric induced delays ρ_{atm} (ionospheric and tropospheric effects); instrumental components ρ_{ins} (clock errors, sub-system delays, antenna offsets); and noise n [9]:

$$\rho = \rho_{\text{geo}} + \rho_{\text{atm}} + \rho_{\text{ins}} + n \quad (2.1)$$

The delays are usually given in the time domain, but they can be also given as ranges, in the space domain, multiplying by the speed of light. In this chapter, range and delay will be both understood as in units of length.

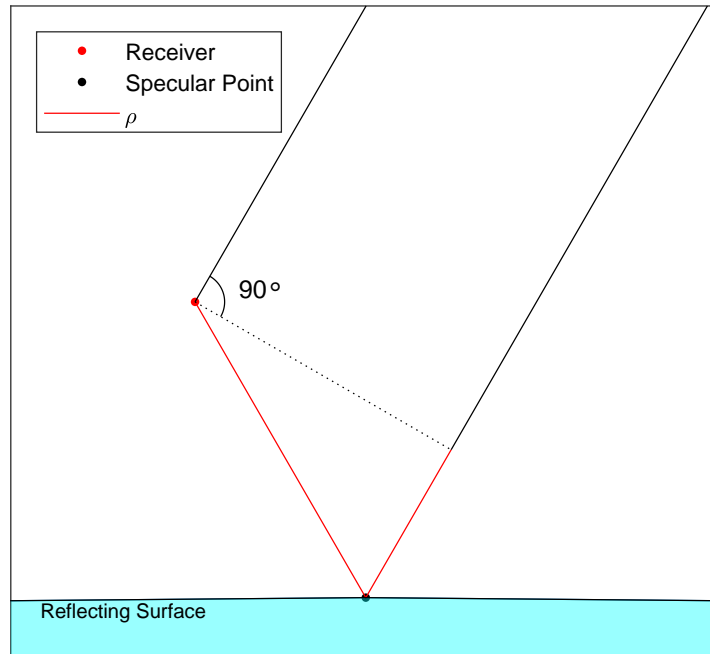


Figure 2.3: Delay between the Transmitter and the Receiver

2.2.1 Geometric Delay ρ_{geo}

ρ_{geo} is the geometric distance between the reflected and direct raypaths, if they both were collected at the well-positioned up-looking antenna. It depends on geometric parameters such as the altitude of the receiver above the reflecting surface and the elevation angle of the observation. Of course we could rewrite Equ. (2.1), use the measured altimetric range and other delays to express the geometric delay:

$$\rho_{\text{geo}} = \rho - \rho_{\text{atm}} - \rho_{\text{ins}} - n \quad (2.2)$$

2.2.2 Atmospheric Delay ρ_{atm}

The atmospheric corrections generally applied to GNSS navigation data are related to tropospheric and ionospheric effects. For GNSS-R at relatively low altitudes (such as the campaign presented in chapter 3), the ionospheric ones can be neglected, since both direct and reflected radio links are similarly effected. General models for the tropospheric delay induced in GNSS-like signals are given in the work by e.g. McCarthy and Petit [14] and Spilker et al. [10], where the effect of the troposphere onto the GNSS delay is a function of several meteorological parameters. However, the delays induced by the troposphere layer above the receiving platform cancel out, and only those due to the bottom layer, between the surface and the receiver, affect the altimetric range (Obviously, this assumption fails for orbiting receivers.).

The variable Atmospheric Delay included in the provided integrated data in chapter 3 is a simple model for ρ_{atm} , given in meters:

$$\rho_{\text{atm}} = \frac{4.6}{\sin(e)} \left(1 - e^{-\frac{H}{8621}}\right) \quad (2.3)$$

where H is the altitude of the receiver above the reflecting surface, e is the elevation angle.

More complex models are given by Niell [16], but they should be correct to include solely twice the contribution below the receiver altitude.

2.2.3 Instrument Delay ρ_{ins}

ρ_{ins} includes instrumental biases, such as residual clock effects, cable lengths and the antenna's offset vector (3-D vector between the up- and down-looking antennas).

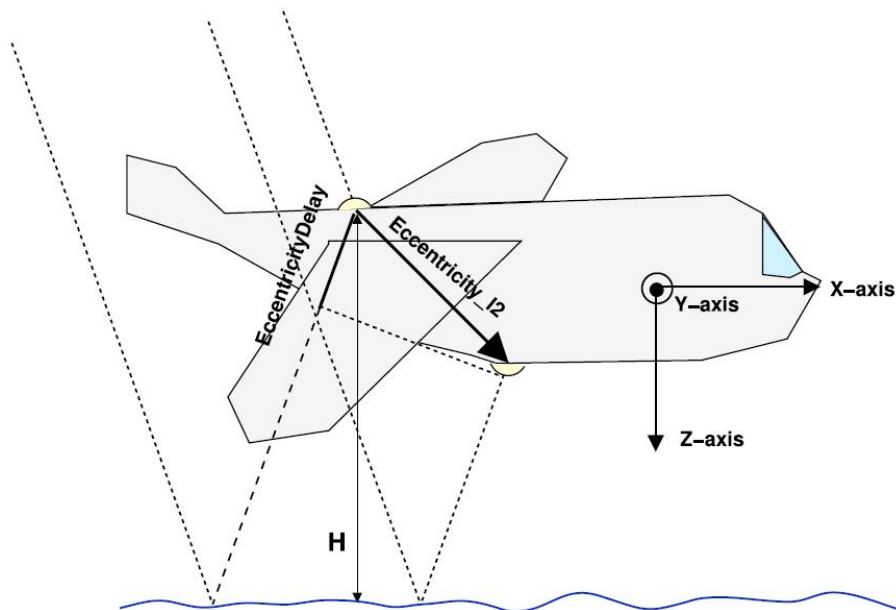


Figure 2.4: Sketch of the Body Frame Coordinate System used to provide the Offset between Antennas [11]

2.2.3.1 Eccentricity Delay

For the flight discussed in chapter 3 the antenna's offset vectors are provided as global attributes and are given in the body frame reference system defined in figure 2.4. Table 2.2 is the data of the first flight discussed in chapter 3.

Antenna	Offset Vectors [m]
Up-looking antenna	(0.125, -0.391, 1.590)
Down-looking antenna	(0.087, 0.510, 1.661)

Table 2.2: Example of the Offset Vectors (First Flight on 13.07.05)

In the integrated data in chapter 3, the projection of these vectors into the direction of the observation is given in the variable Eccentricity Delay, in meters. Note that due to different azimuths and elevation angles of observations, simultaneous observations from different satellites correspond to different values of this delay. Its convention sign is defined so that it must be subtracted to the measured altimetric range to obtain the total delay between the direct raypath and the reflected raypath that would have been received at the up-looking antenna position.

2.3 Specular Point Height Estimation Method

2.3.1 Determine the Position of Transmitter and Receiver

In order to solve the altimetric problem, an accurate knowledge of the position of both transmitter's and receiver's antennas' phase centers are required, expressed as their 3D vector with respect to the center of the Earth (see figure 2.1).

We assume that both can be obtained, Precise Orbit Determination of the GNSS transmitters and GNSS-based plus Inertial Navigation Systems (or others) for the receiver. Both of them are measured in the earth-centered earth-fixed (ECEF) coordinate system.

In some cases it might also be interesting to extract the receiver's altitude with respect to a reference height.

2.3.2 The 2-D Position (Longitude and Latitude) on the Ellipsoid Surface

Before the 3-D position determination, it is necessary to introduce a method to find the 2-D position of a point which located on the surface of the ellipsoid as a function of transmitter position and receiver position. The 2-D position here means the longitude and the latitude of a point in geodetic coordinate system, the ellipsoidal height is zero, although the coordinates in ECEF coordinate system has 3 components.

Besides the position of the transmitter and the receiver another important given quantity is the size and form of the Earth, in other words, the reference ellipsoid. Two parameters here are needed: the equatorial radius R_E and the flattening f (or the eccentricity e), this two parameters in WGS84 are:

$$\text{Equatorial Radius : } R_E = 6\,378.137 \text{ km} \quad (2.4)$$

$$\text{Flattening : } f = \frac{1}{298.257\,223\,563} \quad , \quad (e = \sqrt{2f - f^2} = 0.081\,819\,190\,842\,62) \quad (2.5)$$

The input of this algorithm are the receiver (\mathbf{R}) and transmitter (\mathbf{T}) position in ECEF coordinate system:

$$\mathbf{R} = \begin{bmatrix} R_x \\ R_y \\ R_z \end{bmatrix} , \quad \mathbf{T} = \begin{bmatrix} T_x \\ T_y \\ T_z \end{bmatrix} \quad (2.6)$$

First of all, it is necessary to make an initial guess of the 2-D position, let's say, the projection of the receiver position onto the surface of the ellipsoid (point S_0 in figure 2.5):

$$\mathbf{S}_0 = \frac{\mathbf{R}}{\text{norm}(\mathbf{R})} r_0 \quad (2.7)$$

where r_0 is the radius length of the Earth on that point with the origin at the center of the ellipsoid, it is a value which only depends on the latitude ϕ . Of course it can be calculated if the coordinates of a point are provided. The derivation process is as follows:

The vector from the ellipsoid center to an arbitrary point on the ellipsoid surface is:

$$\mathbf{r} = \begin{bmatrix} X \\ Y \\ Z \end{bmatrix} \quad (2.8)$$

The latitude angle of this point is:

$$\phi = \arcsin \frac{|Z|}{\text{norm}(\mathbf{r})} \quad (2.9)$$

If cartesian coordinates are introduced such that the origin is the center of the ellipse and the x-axis is the major axis we obtain the equation of the ellipse:

$$\frac{x^2}{a^2} + \frac{y^2}{b^2} = 1 \quad (2.10)$$

The shape parameters a , b are called the semi-major and semi-minor axes.

Using the sine and cosine functions, a parametric representation of the ellipse above in polar coordinate system can be obtained:

$$\begin{bmatrix} x \\ y \end{bmatrix} = \begin{bmatrix} r \cos \phi \\ r \sin \phi \end{bmatrix} \quad (2.11)$$

Take Equ. (2.11) into Equ. (2.10) we have:

$$\frac{r^2 \cos^2 \phi}{a^2} + \frac{r^2 \sin^2 \phi}{b^2} = 1 \quad (2.12)$$

The equation above can be rewritten as:

$$r^2(b^2 \cos^2 \phi + a^2 \sin^2 \phi) = a^2 b^2 \quad (2.13)$$

Now the radius r can be expressed as a function of ϕ :

$$r(\phi) = \frac{ab}{\sqrt{a^2 \sin^2 \phi + b^2 \cos^2 \phi}} = \frac{a}{\sqrt{\frac{a^2}{b^2} \sin^2 \phi + \cos^2 \phi}} \quad (2.14)$$

Using $b^2 = a^2(1 - e^2)$ the equation above could be simplified as follows:

$$r(\phi) = \frac{a}{\sqrt{\frac{1}{1-e^2} \sin^2 \phi + \cos^2 \phi}} = \frac{a}{\sqrt{\frac{1-\cos^2 \phi}{1-e^2} + \cos^2 \phi}} = \frac{a}{\sqrt{\frac{1-e^2 \cos^2 \phi}{1-e^2}}} \quad (2.15)$$

Finally we get the radius length of an arbitrary point on an ellipsoid surface:

$$r = a \sqrt{\frac{1 - e^2}{1 - e^2 \cos^2 \phi}} \quad , \quad \text{with } \phi = \arcsin\left(\frac{|\mathbf{Z}|}{\sqrt{|\mathbf{X}|^2 + |\mathbf{Y}|^2 + |\mathbf{Z}|^2}}\right) \quad (2.16)$$

Next, after we have the initial value, an iterative method is designed to solve the problem:

Step 1. Calculate the correction direction:

$$\mathbf{d}_{XYZ} = \frac{\mathbf{R} - \mathbf{S}_i}{\text{norm}(\mathbf{R} - \mathbf{S}_i)} + \frac{\mathbf{T} - \mathbf{S}_i}{\text{norm}(\mathbf{T} - \mathbf{S}_i)} \quad (2.17)$$

Step 2. Apply the raw correction:

$$\mathbf{S}_{c,i+1} = \mathbf{S}_i + k \cdot \mathbf{d}_{XYZ} \quad (2.18)$$

where k is the correction gain, the value should neither be too small (cause unnecessarily too many times of iteration) nor too large. It's more or less depends on the length of each move after each iteration, that is from \mathbf{S}_i to \mathbf{S}_{i+1} . So the value at very beginning could set to such as 10 km, after several loop when we get closer then the correction gain should also have a smaller value accordingly.

Step 3. Constrain to Earth surface:

$$\mathbf{S}_{i+1} = \frac{\mathbf{S}_{c,i+1}}{\text{norm}(\mathbf{S}_{c,i+1})} r_{i+1} \quad (2.19)$$

$$\text{with } r_{i+1} = a \sqrt{\frac{1 - e^2}{1 - e^2 \cos^2 \phi_{i+1}}} \quad , \quad \phi_{i+1} = \arcsin\left(\frac{|\mathbf{Z}_{i+1}|}{\sqrt{|\mathbf{X}_{i+1}|^2 + |\mathbf{Y}_{i+1}|^2 + |\mathbf{Z}_{i+1}|^2}}\right) \quad (2.20)$$

The iterative routine stops when the move from \mathbf{S}_i to \mathbf{S}_{i+1} become smaller than a predetermined tolerance, for example 1 mm. Figure 2.5 shows how the point according to the iterative method described above from the initial guess \mathbf{S}_0 move to the right position.

In order to get the 2-D position (longitude and latitude), it needs simply a coordinate transformation, from cartesian to ellipsoidal. It requires another iterative method described below:

The coordinates of a point on the ellipsoid surface in cartesian coordinate system are (Note the h here has the value 0 if the point lies on the Earth ellipsoid surface):

$$x = (N + h) \cos \phi \cos \lambda \quad (2.21)$$

$$y = (N + h) \cos \phi \sin \lambda \quad (2.22)$$

$$z = (N(1 - e^2) + h) \sin \phi \quad (2.23)$$

with

$$N = \frac{a}{\sqrt{1 - e^2 \sin^2 \phi}} \quad (2.24)$$

is the normal rad curvature of the ellipse and λ is the longitude.

From Eqn. (2.21) and Eqn. (2.22) we have:

$$\lambda = \arctan\left(\frac{y}{x}\right), \quad (2.25)$$

$$\text{and } h = \frac{\sqrt{x^2 + y^2}}{\cos \phi} - N \quad (2.26)$$

From Eqn. (2.21), Eqn. (2.22) and Eqn. (2.23) we have:

$$\phi = \arctan\left(\frac{z}{\sqrt{x^2 + y^2} \frac{(N + h)}{(N(1 - e^2) + h)}}\right) \quad (2.27)$$

Eqn. (2.26) and Eqn. (2.27) must be solved simultaneously and iteratively. The rate of this convergence is very high because in general H is much smaller than N [13].

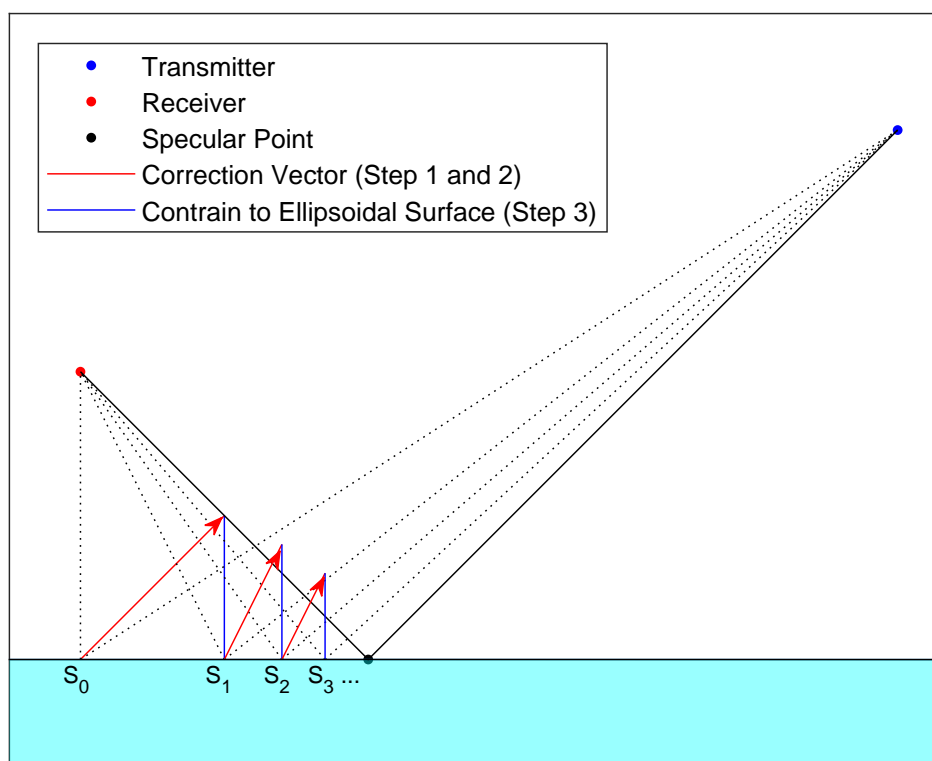


Figure 2.5: Find the Specular Point for 2-D Circumstance

2.3.3 The 3-D Position (Longitude, Latitude and ell. Height) of the Specular Point

As shown in figure 2.6, the Sea Surface Height (SSH) is calculated relative to the surface of the theoretical Earth ellipsoid in the WGS84 system, which has zero altitude. A two-loop iterative method for SSH calculation can be employed, which is described below.

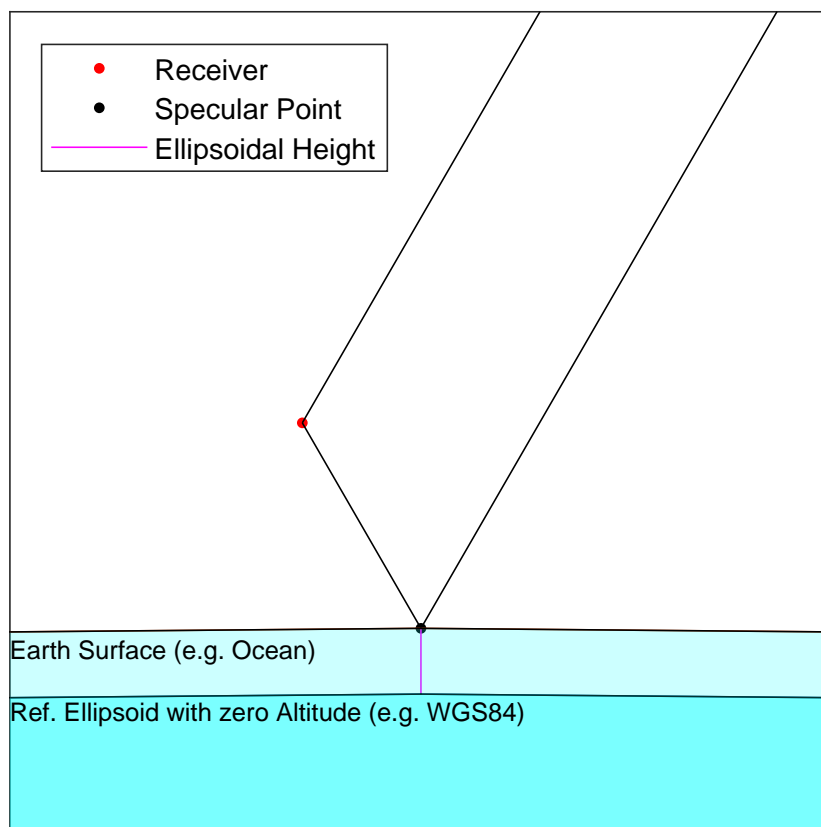


Figure 2.6: Geometry of the Receiver, Earth Ellipsoid, Sea Surface, direct and reflected Signal Paths

Figure 2.7 shows the flowchart of how to calculate the SSH. Specifically, for a given tentative SPP guess, since both the GNSS satellite position (x_t, y_t, z_t) and the receiver position (x_r, y_r, z_r) are known, the specular point position (SPP) (x_s, y_s, z_s) on the tentative sea surface can be readily determined [18].

The total path length (TPL) from the satellite through the tentative SPP and to the receiver is given by:

$$\tilde{R}_{tsr} = \tilde{R}_{ts} + \tilde{R}_{sr} \quad (2.28)$$

where

$$\tilde{R}_{ts} = \sqrt{(x_t - \tilde{x}_s)^2 + (y_t - \tilde{y}_s)^2 + (z_t - \tilde{z}_s)^2} \quad (2.29)$$

$$\tilde{R}_{sr} = \sqrt{(x_r - \tilde{x}_s)^2 + (y_r - \tilde{y}_s)^2 + (z_r - \tilde{z}_s)^2} \quad (2.30)$$

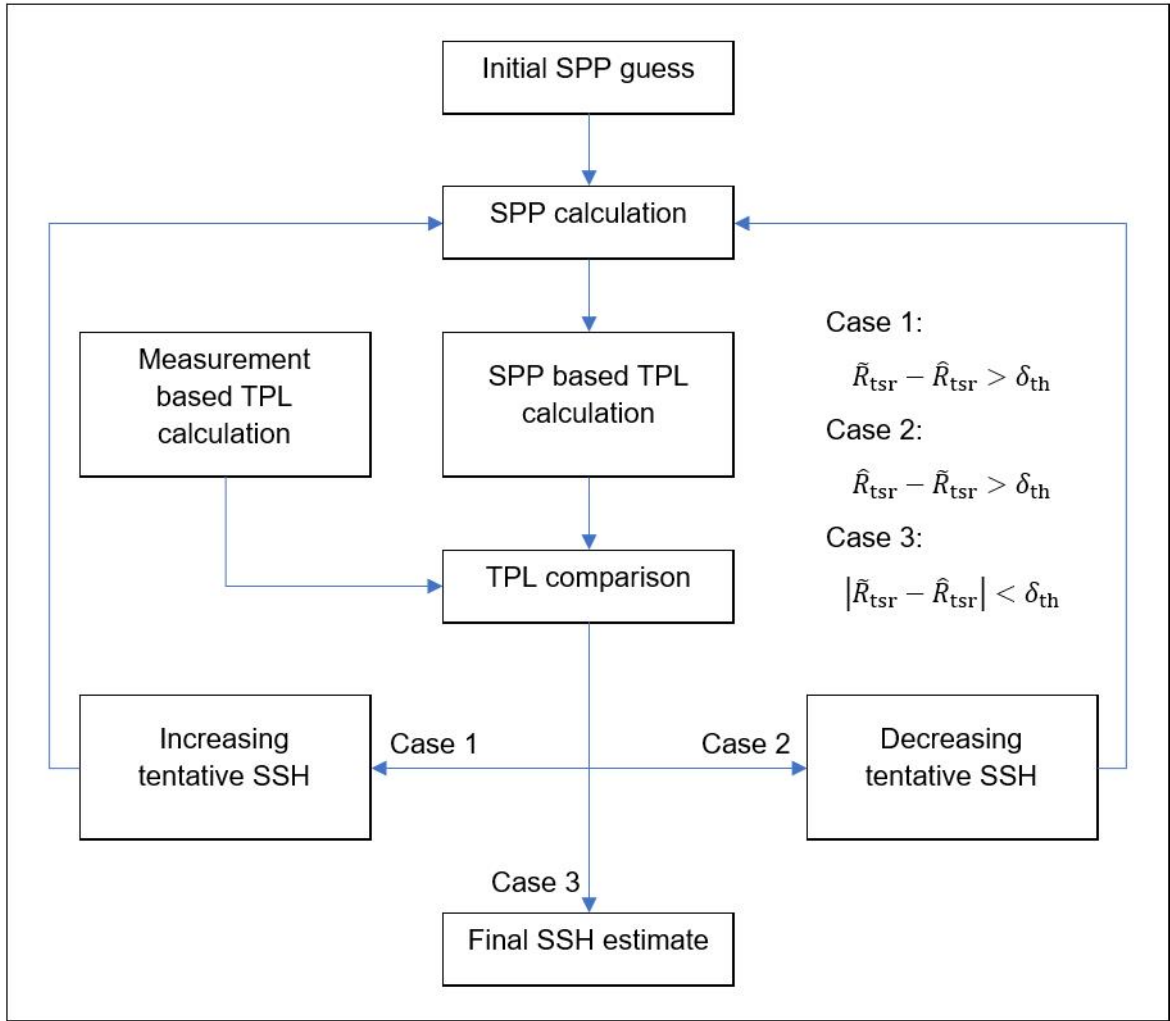


Figure 2.7: Flowchart of the SSH Calculation

On the other hand the TPL can also be estimated using the relative propagation time delay (τ) between the direct signal and the reflected signal:

$$\hat{R}_{tsr} = R_{tr} + c \cdot \tau \quad (2.31)$$

where c is the speed of light, τ is the estimated relative time delay and

$$R_{tr} = \sqrt{(x_t - x_r)^2 + (y_t - y_r)^2 + (z_t - z_r)^2} \quad (2.32)$$

Note that the second term on the right side of Eqn. (2.31) is equal to the geometric delay ρ_{geo} mentioned in section 2.2.

Then, as indicated in figure 2.7, the calculated TPL by Eqn. (2.28) is compared with the measured TPL by Eqn. (2.31) to determine whether the tentative sea surface height h should be increased or decreased.

To reduce the computational complexity of the iterative method, a simple technique may be used. For instance, if $\tilde{R}_{\text{tsr}} > \hat{R}_{\text{tsr}}$, it means the tentative surface height h is lower than the true value and because of the special geometric contribution of the transmitter, specular point and the receiver ($|R_{\text{ts}}| \gg |R_{\text{rs}}|$) the h should be increased by an increment roughly equal

$$\frac{\sin e}{2} (\tilde{R}_{\text{tsr}} - \hat{R}_{\text{tsr}}) \quad (2.33)$$

where e is the elevation angle. The illustration below gives an explanation of how the height is estimated. With this trick we could already estimate approximate 90% of the height after the first iteration, and we could reach an accuracy of a smaller order of magnitude after each next iteration (e.g. the ell. height is 50 m, $\Delta h_1 \approx 45$ m, $\Delta h_2 \approx 4.5$ m, $\Delta h_3 \approx 0.45$ m... so after about 6 times of iteration we could reach the true specular point height with an accuracy of 1 mm).

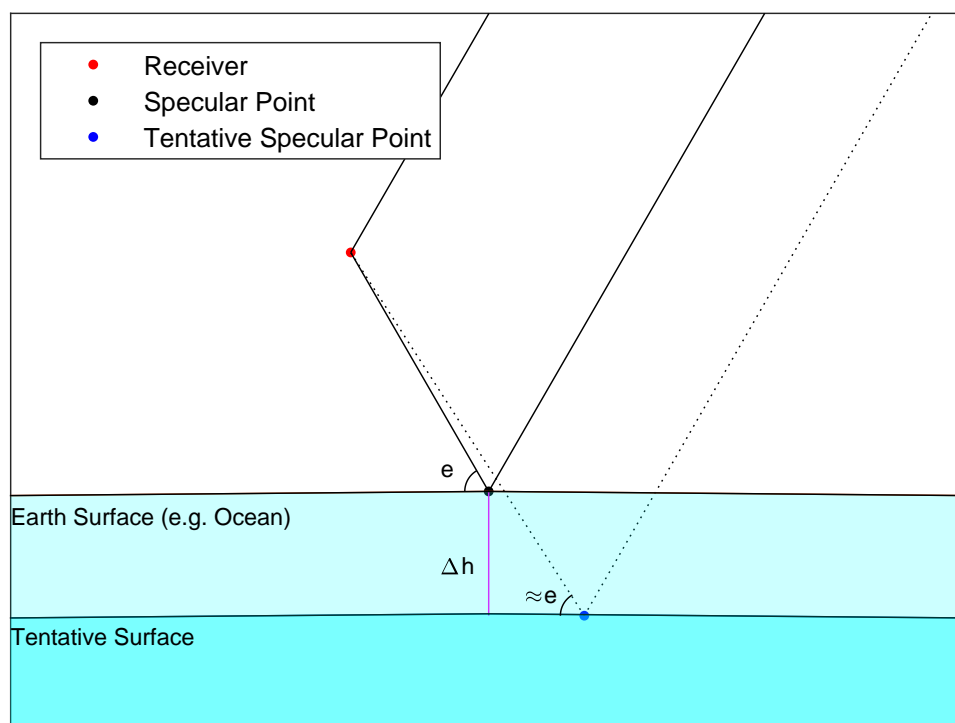


Figure 2.8: Explanation of the Height Estimate Update

After each iteration we get a new tentative sea surface height h (or the height increment Δh_i), with this value we can calculate a new tentative SSP with the method introduced in section 2.6.2. Note that the only change in section 2.3.2 has to be done is the Eqn. (2.19), the new one is:

$$\mathbf{S}_{i+1} = \frac{\mathbf{S}_{c,i+1}}{\text{norm}(\mathbf{S}_{c,i+1})} (r_{i+1} + \Delta h_i) \quad (2.34)$$

The process terminates once the difference between the two TPLs is smaller than the predefined threshold δ_{th} , e.g. 1 mm.

2.3.4 Summary

In this section the specular point position is determined via a method with two iterative algorithms, one for the ellipsoidal height (normal direction) and the other for the longitude/latitude (horizontal direction). The initial value is the point direct under the receiver on the ellipsoid surface. We started the calculation from here and firstly found a tentative SPP on the Earth ellipsoid. After that we elevate this tentative specular point to another level parallel to the Earth ellipsoid surface. Next, we determine a new SPP on this new level... Figure 2.9 illustrates the whole procedure of this method.

It is a remarkable fact that the estimated ellipsoid height is not the sum of each Δh_i , although it's not far from what we want, because each of them is calculated at a different location (longitude/latitude). The specular point location and height is determined via Eqn. (2.25), Eqn. (2.26) and Eqn. (2.27) after the last iteration (when termination criterion satisfied).

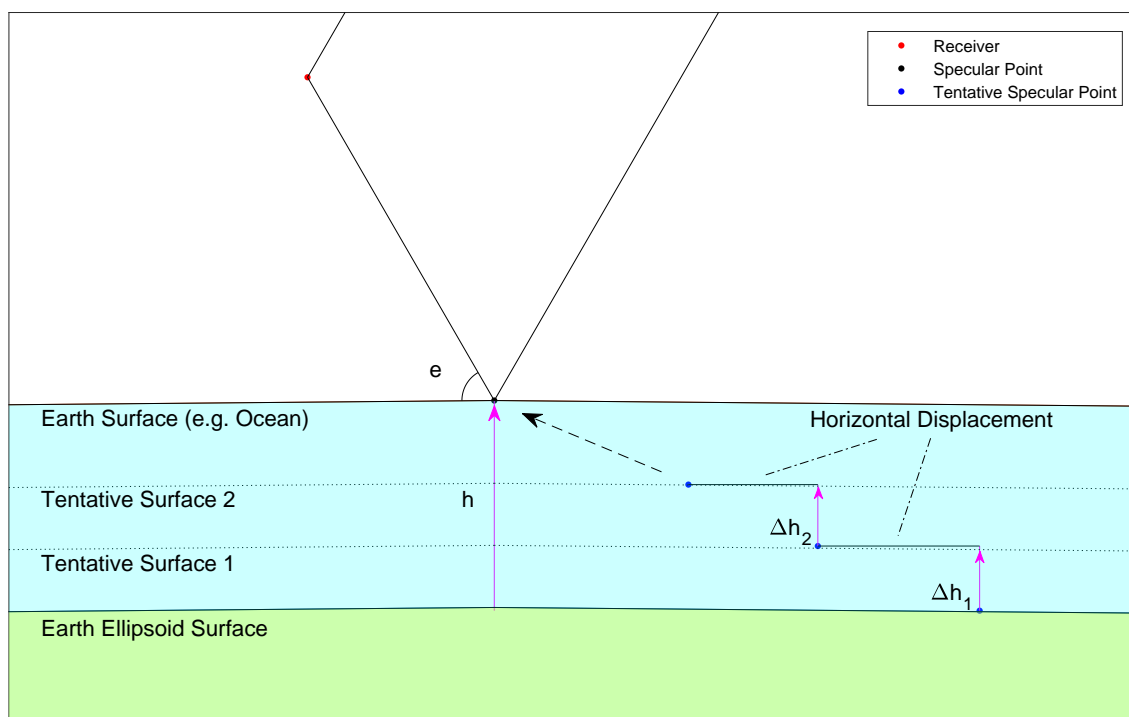


Figure 2.9: Summary of the Method

Chapter 3

A Specific Example

3.1 Data Sources: GOLD_RTR Mining

GOLD-RTR Mining is a web server for downloading GNSS-R experimental data and related information. The data was collected from 2005 to 2012 with the ICE/IEEC-CSIC's designed and manufactured GPS Open-Loop Differential Real-Time Receiver (GOLD-RTR).

Since 2005, when the GOLD-RTR was tested on two air-borne campaigns, Global Navigation Satellite System Reflections (GNSS-R) have been obtained with this dedicated receiver. More than 40 flights have been conducted so far, over oceans, lakes and land; and more than 250 days of continuous monitoring of sea, ice and dry snow. The uniqueness of the data set, consisting of both integrated (Up to a certain preprocessing level, but they do not provide the final geophysical products.) and also complex raw data; measuring the co- and cross-polar components of the reflected scattering; with delay and delay-Doppler maps, makes it suitable for testing a noticeable amount of potential applications and techniques [4].

All these data sets, together with the information necessary to understand and analyze them, are made available through this server. The table below gives an overall summary of each campaign and the map below shows the location of the tracks of the reflected signals captured in different campaigns [2].

Campaign:	Year:	Funded by:	Geographic area:	Air/Ground	Ocean/Land/Ice/Snow:	LHCP+RHCP reflections:	Receiver:
Gold Test	2005	IEEC/ICC	NW Mediterranean Sea (Spain)	A (3 flights)	O/L	yes	GOLD-RTR (clean-replica)
CoSMOS-OS	2006	ESA	North Sea (Norway)	A (12 flights)	O	yes	GOLD-RTR (clean-replica)
CoSMOS-OS	2007	ESA	Baltic Sea (Finland)	A (2 flights)	O	no	GOLD-RTR (clean-replica)
CAROLS	2007	CNES	South France, Bay Biscay (France)	A (3 flights)	O/L	yes	GOLD-RTR (clean-replica)
SMOS Calibration Rehearsal Campaign	2008	ESA	Finland to Valencia (Europe)	A (12 flights)	O/L	no	GOLD-RTR (clean-replica)
CAROLS	2009	CNES	South France, Bay Biscay (France), Valencia area (Spain)	A (11 flights)	O/L	yes	GOLD-RTR (clean-replica)
GPS-SI	2008-2009	ESA	Disko Bay (Greenland)	G (7 months)	O/I/S	yes	GOLD-RTR (clean-replica)
GPS-DS	2009	ESA	Dome-C (Antarctica)	G (10 days)	S	yes	GOLD-RTR (clean-replica)
PIT-POC 2	2011	ESA	Baltic Sea (Finland)	A (2 flights)	O	yes	PIRA (interferometric)
Begur	2012	ESA	NW Mediterranean (Spain)	G (3 days)	O	yes	PARIS-MB (interferometric)

Figure 3.1: Overall Summary of each Campaign

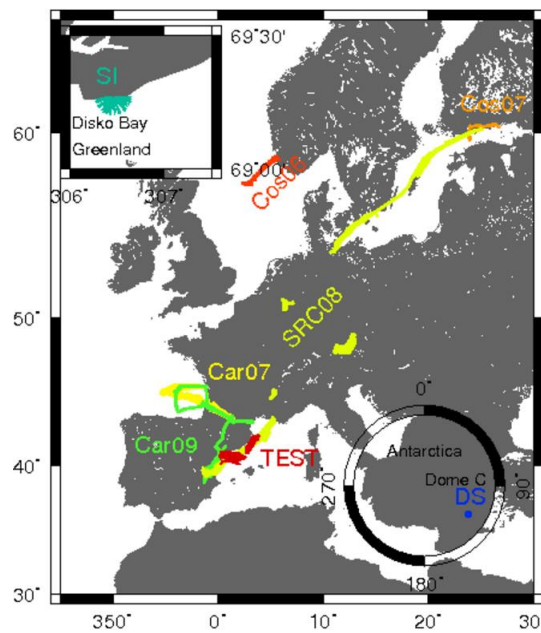


Figure 3.2: Tracks of the reflected Signals captured in different Campaigns

3.2 Campaign "Gold Test"

Campaign "Gold Test" refers to a set of three flights carried on by ICE/IEEC-CSIC and ICC in 2005, with the aim of testing the GOLD-RTR GNSS-R instrument during aircraft campaigns.

In the morning of 13.07.2005, a flight over the Mediterranean Sea along the Catalonian north coast was performed. Several configurations were proved, including Delay Maps, Delay Doppler Maps and altimetric tests. The reflected GPS signals were all gathered through LHCP antennas.

During 14.07 two flights were performed. The first one overflew the Ebre's delta and entered several kilometers into the sea, repeating this process few times. Similar configurations were proved, but in addition, the reflected GPS signals were gathered through both RHCP and LHCP antennas for some time periods. During the afternoon, a flight with the same pattern and configurations that the day before was done [1].

A detailed introduction and comparison of the flight on 13.07 and the second flight on 14.07 is tackled in section 3.2.1, 3.2.2 and 3.2.3, because both of them flew over a same piece of area.



Figure 3.3: The Aircraft and the Hardware applied during the Measurement

3.2.1 Observations

Let's first have a look at the observations provided from this campaign:

Time

The time applied during the measurement is the GPS time (Global Positioning System time). It is the atomic time scale implemented by the atomic clocks in the GPS ground control stations and the GPS satellites themselves. GPS time was zero at 0h 06.01.1980 (Sunday, the first day of a GPS week) and since it is not perturbed by the leap seconds, the GPS time was ahead of UTC by 13 seconds at the time of the measurement (from 01.01.1999 to 01.01.2006) [5].

The GPS time is given in week and second, e.g. the GPS week of this campaign was 1331 and the first GPS second of the first and the third flight was 294554 and 399934. It's easy to convert it into weekday, hour, minute and second in UTC and local time:

	GPS	UTC	Local
Begin of 13.07 /Wed.	09:49:14	09:49:01	11:49:01
Begin of 14.07 /Thu.	15:05:34	15:05:21	17:05:21

Table 3.1: The Time at the Begin of the Measurement of each Flight

PRN

Pseudorandom noise (PRN) codes are the important element of code division multiple access (CDMA) based satellite navigation systems. Each satellite within a GNSS constellation has a unique PRN code that it transmits as part of the C/A navigation message. This code allows any receiver to identify exactly which satellite(s) it is receiving.

We can see from figure 3.4, that there are altogether 9 satellites used during the measurement on the first day (PRN = 2, 4, 8, 10, 13, 20, 23, 24, 27) and 8 used on the second day (PRN = 7, 8, 9, 10, 18, 26, 28, 29).

Besides, we notice that there are always 5 connections at one time (e.g. on 13.07, from measurement begin to 1000 sec., PRN = 4, 13, 20, 23 and 24 are used). Another satellite will be connected immediately if one connection stopped, interrupted or the satellite just moves out of sight from the view of the receiver (e.g. number 27 replaced number 20). This is because that the plane is equipped with a receiver with 10 channels and the receiver get from each satellite 2 links (a direct link and a reflected link).

In fact the number of the satellite available in a specific place and time especially nowadays with fully operational GNSS transmitters (GPS and GLONASS) is much more than that. It is easy to capture signals from 15 to 25 GNSS sources simultaneously using a receiver on the

Earth surface (see figure 3.5). This number increases with the altitude of the receiver. Moreover, this number will steadily increase with the deployment of new constellations: the European GALILEO, the Chinese COMPASS/Beidou and regional constellations (Indian IRNSS and Japanese QZSS...). All together will provide more than 100 GNSS transmitters globally distributed. However, the hardware in this campaign allows only a limited number of usage. And we prefer the satellite with higher elevation in order to improve the measurement accuracy. Of course if the plane were equipped with a receiver with more channels then the number of the measurement would increase accordingly. It means more data would be collected per unit time / flight, it's not only more efficient but also more economical.

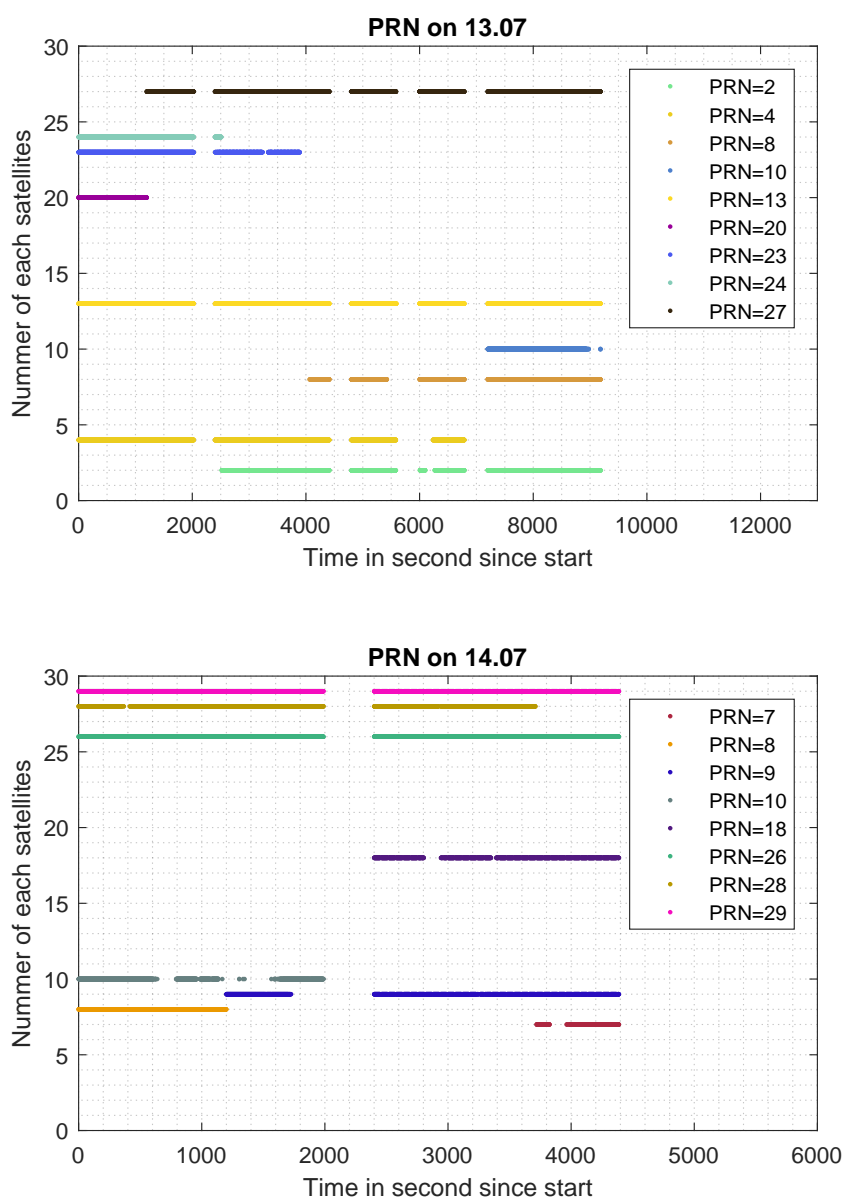


Figure 3.4: Satellites used during the Measurements

Figure 3.5 gives the frequency percentage of simultaneously visible GNSS transmitters from a receiver located at the surface-level, and mid latitude (45°). Statistics performed with real orbits corresponding to the GPS and GLONASS constellations as on 18.03.2012. These numbers would increase for reflected signals from a receiver at higher altitude.

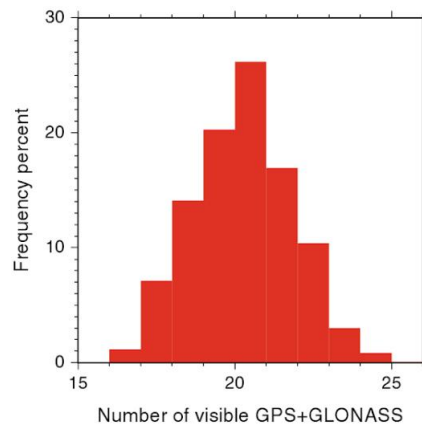


Figure 3.5: The Frequency Percentage of simultaneously visible GNSS Transmitters from a Receiver [11]

Elevation

The elevation angle (complementary of the incidence angle) is the angle between the horizontal plane and the connecting line specular point - transmitter, measured in the vertical plane. The reference direction (i.e. the elevation of zero degree) is a horizontal line in the direction to the horizon, starting from the antenna. The elevation angle is denoted by letter e and has a value between 0 and 90 degrees.

The satellites that appear near the horizon should be ignored because those at low angles are subject to signal fade and they also pick up more atmospheric noise.

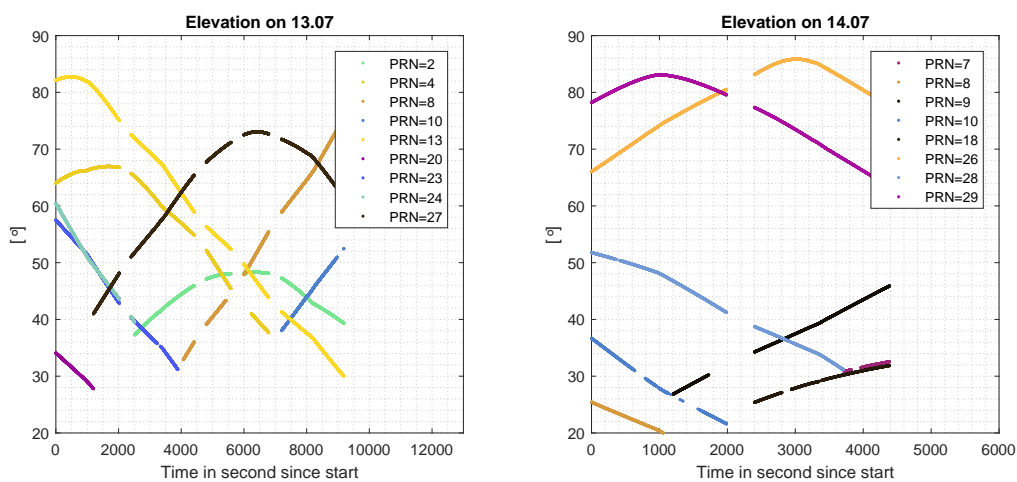


Figure 3.6: The Elevation Angle

Three kinds of Delays

These are the delays mentioned in chapter 2, they are given as ranges.

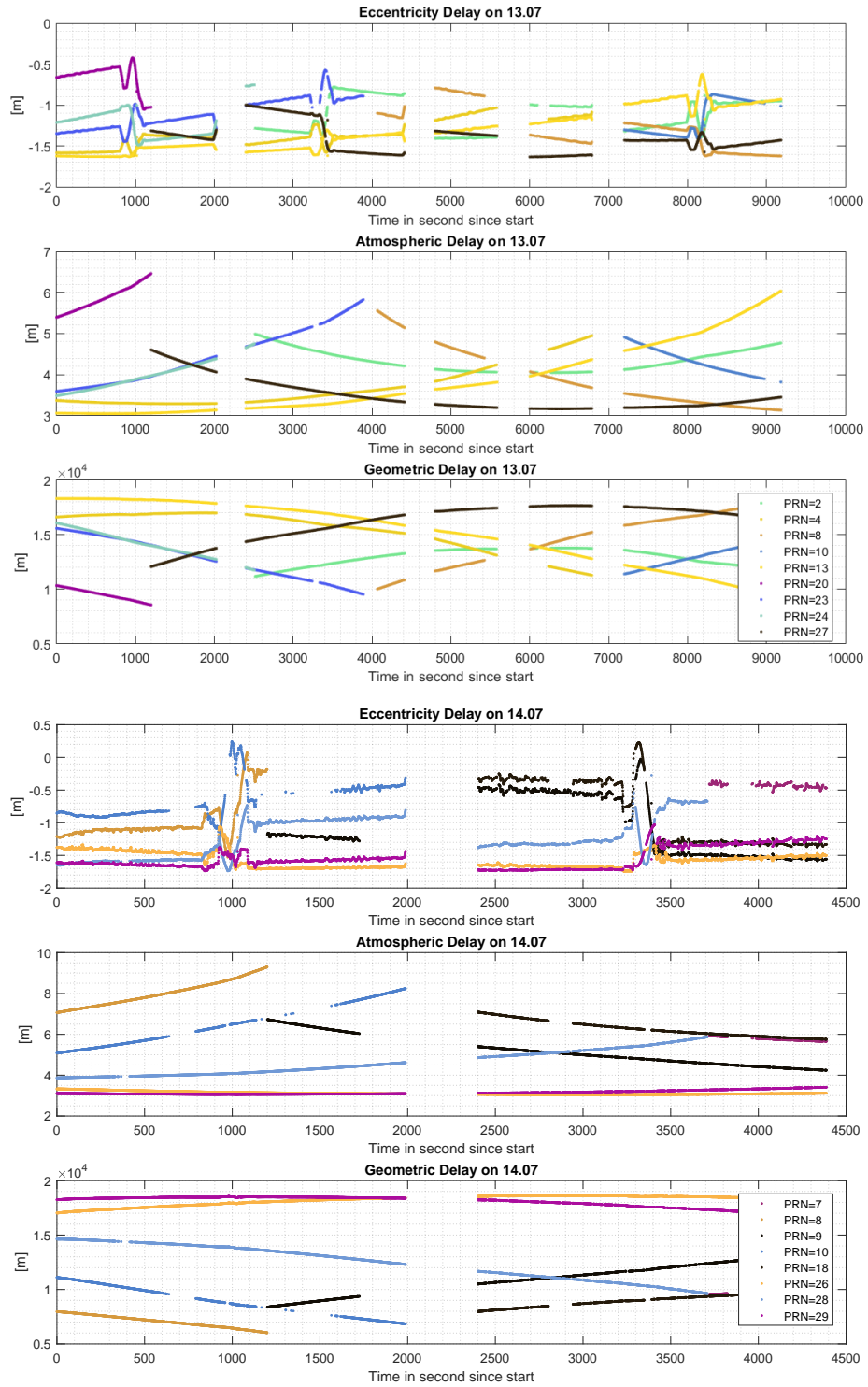


Figure 3.7: The Eccentricity-, atmospheric- and geometric Delay

Receiver Position (given in ECEF Coordinate System):

The flight route is prepared according to the researching area. If the angle of elevation is relative large and the flight altitude is much lower compared to the satellite altitude, then the receiver's location (ground track) is suppose to not far away from the specular point trace.

The figure 3.8 indicates, that the pilot repeated a fast identical air route for several times. This ensure an uninterrupted measurement along the route, considering that the receiver may works not as fluently as expected. In addition, with this repetition we could get a result with denser sampling, in most cases a zonal area. Because each satellite has its own orbit and keeps moving all the time which influence the position of the specular point.

The length of the route is about 140 km for each flight and it's in one direction (Southwest - Northeast). Unfortunately it could probably not deliver a elevation map for a large area.

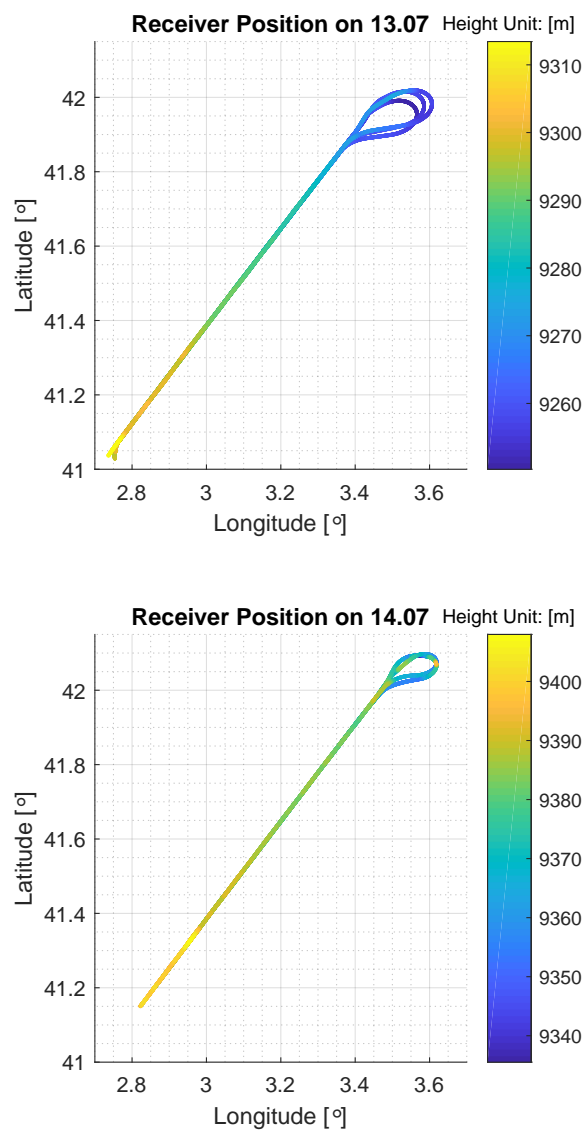


Figure 3.8: The Receiver Position

Transmitter Position (given in ECEF Coordinate System):

Figure 3.9 shows the relative position of the different satellites and the Earth. Note that satellites in this figure are not orbiting the earth in circle, because the coordinate system applied in this plot is not celestial but terrestrial.

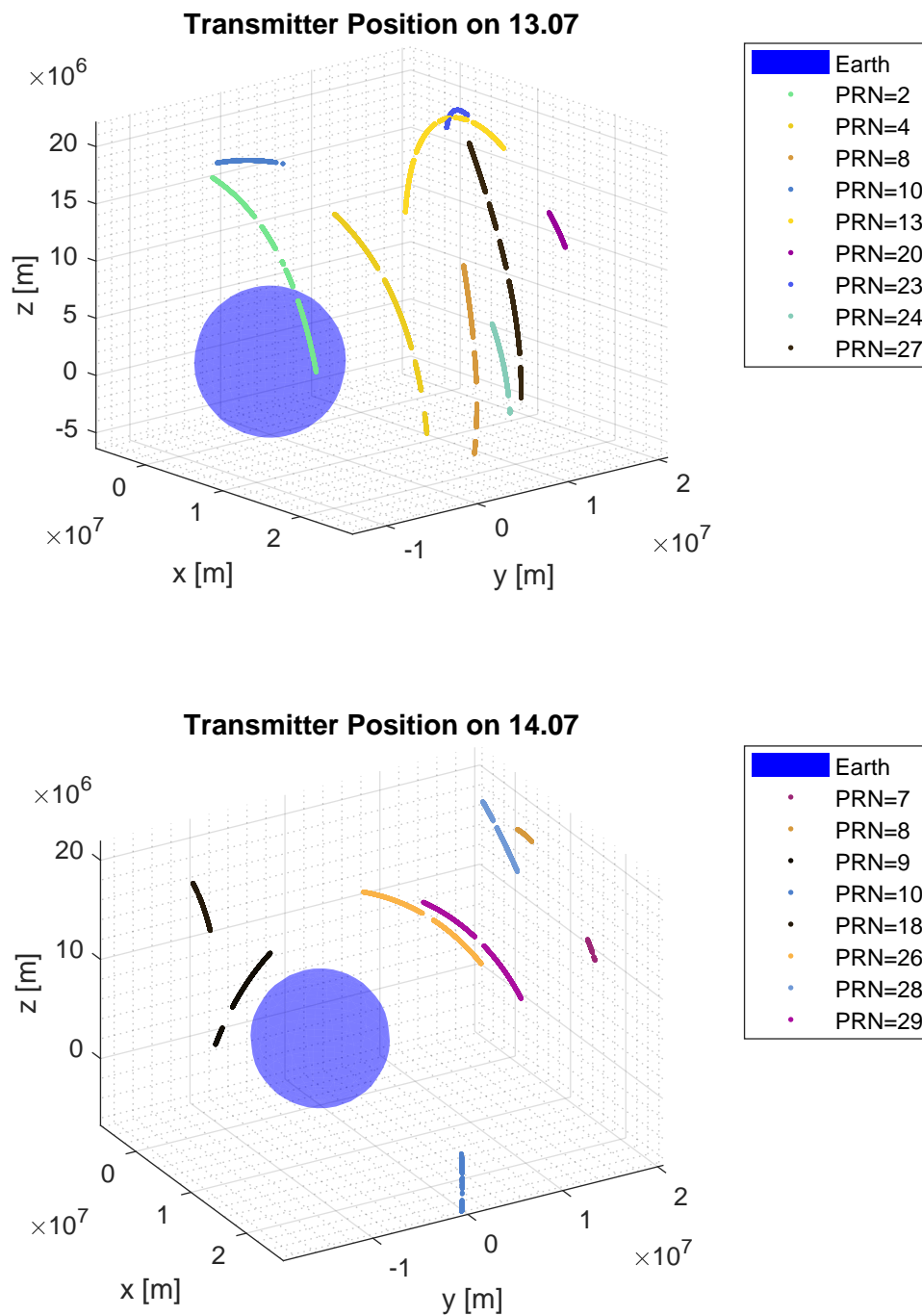


Figure 3.9: The Transmitter Position

3.2.2 The Ellipsoidal Height of the Specular Point

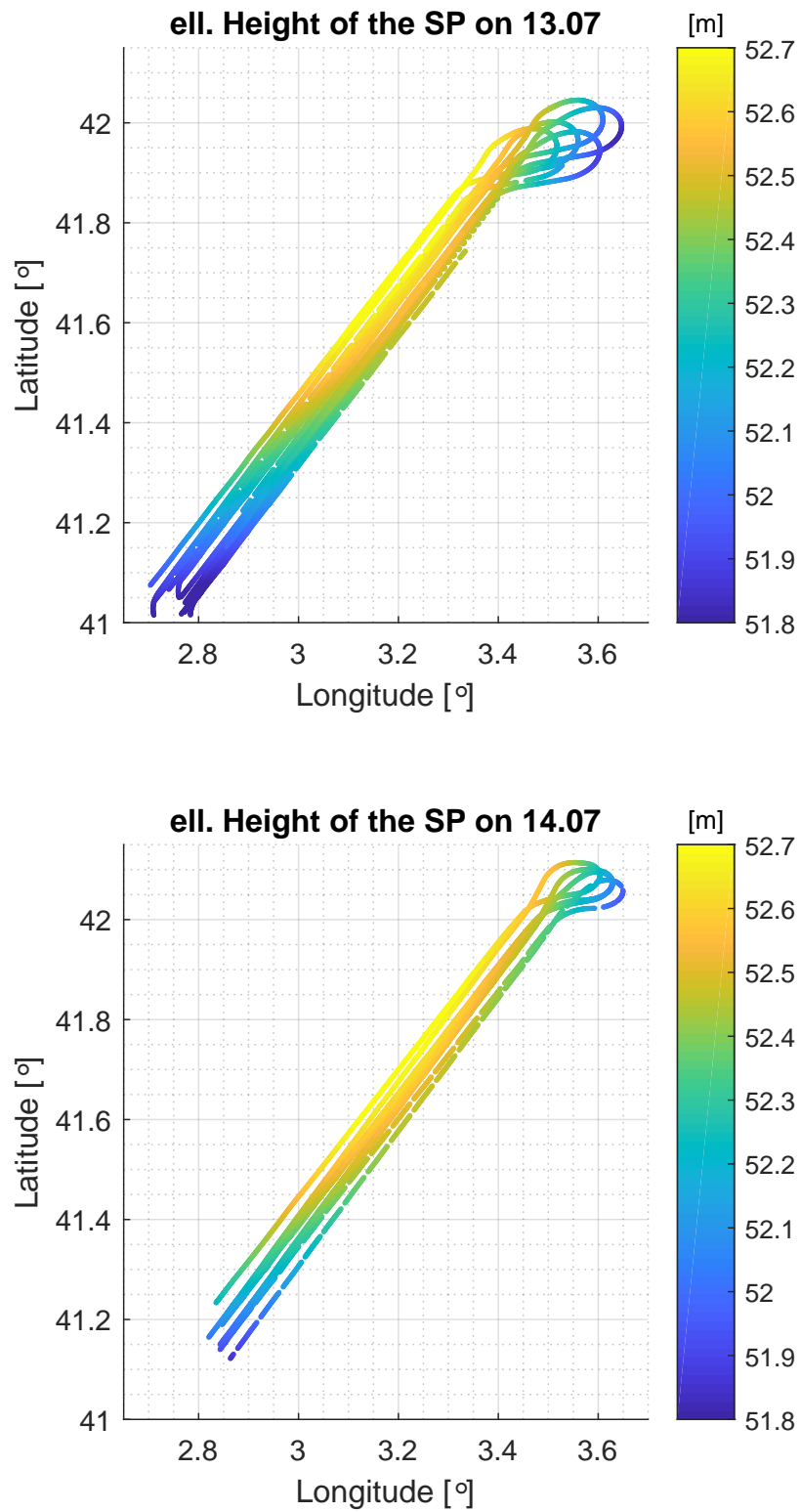


Figure 3.10: The ell. Height of the Specular Point

The ellipsoidal height is solved for each specular point by applying the method introduced in chapter 2. Using the plane coordinate system to express the location (longitude and latitude) and the color bar to show the ell. height we have the figure 3.10. As expected the distribution of the specular point is zonal rather than a narrow line, so it's also possible to analyze the height changes in directions other than the flight direction.

The range of the color bar is set to be the same one in order to compare the two map easier. We can see that in the first day more measurements have been done than the second day and the elevation map looks also better, nevertheless the result of the two days' measurement has a lot of similarities. For example, the middle part of the map (around N41.6°, E3.2°) is approximately 1 meter higher than the both ends, and the area on the Northwest of the route is higher than the Southeast. Perhaps because the coast is just 20 km far from the route on the northwest side and the gravity of the landmass plays a role in forming the sea surface height. To prove this assumption another flight in the region between this one and the coast ought to be carried out.

3.2.3 The Orthometric Height of the Specular Point

The orthometric height of a point is the distance along the curved plumb line (The plumb line differs from the plumb line tendon at 10 km heights by less than 0.01 mm.) from the point to a reference height, for instance, the geoid [7]. Heights outside the geoid is positive. The deviation between the ellipsoidal height h and the orthometric height H is called the geoid undulation N , so we have the equation:

$$N = h - H \quad (3.1)$$

Figure 3.11 indicates the geoid undulation of each specular point, the value ranges from 48 m to 50 m.

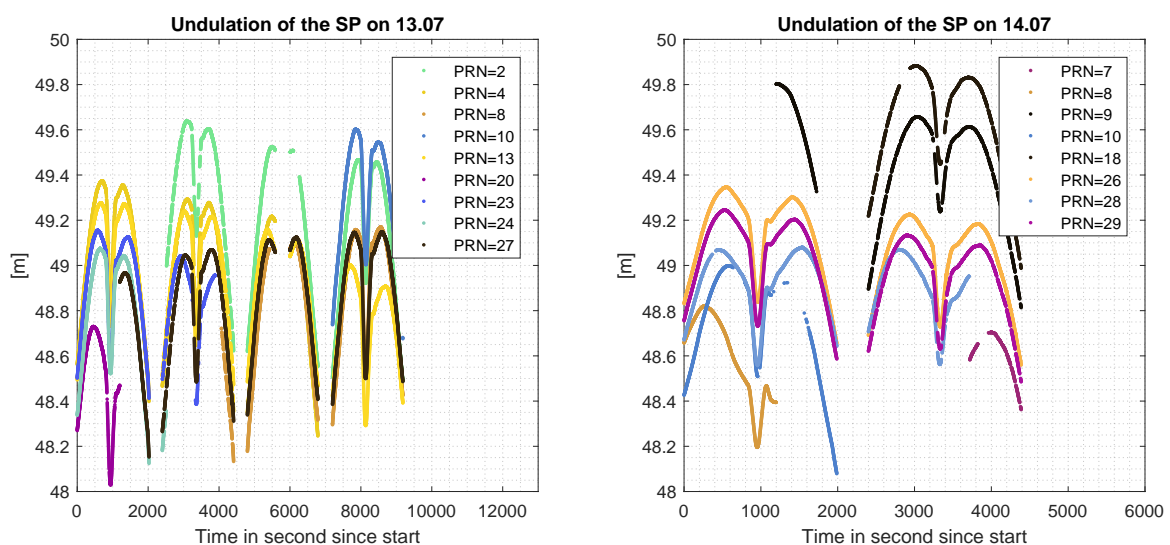


Figure 3.11: The Undulation of the Geoid

With the data above and the equation 3.1 the orthometric height is plotted in figure 3.11, again an identical color bar is applied for both days. The ort. height is about 3.35 meters for both days, and different from the ell. height, the ort. height differs from place to place by no more than 10 cm. However, This result is not astonishing, to a good approximation the geoid is represented by the mean sea level of the oceans in the absence of other influences such as winds and tides.

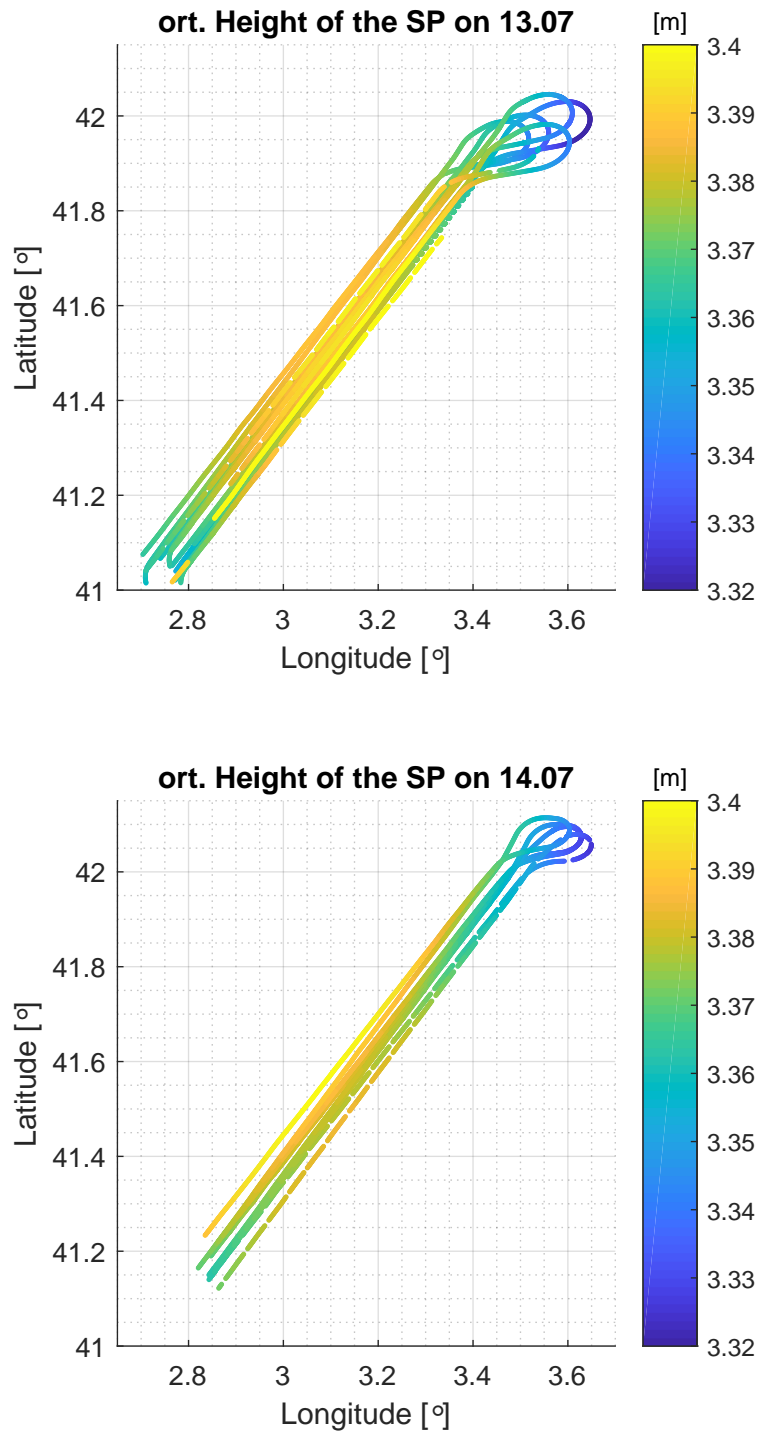


Figure 3.12: The ort. Height of the Specular Point

Due to the inconsistency of the area swept during the two days, it makes more sense if we just focus on a smaller area where have been measured on both days rather than the whole region, e.g. from $N41.4^\circ$ to $N41.6^\circ$ and from $E3.0^\circ$ to $E3.2^\circ$. This is nearly a rectangle with 22 km in length and 17 km in width. The mean height is the average of all the height calculated in this rectangle.

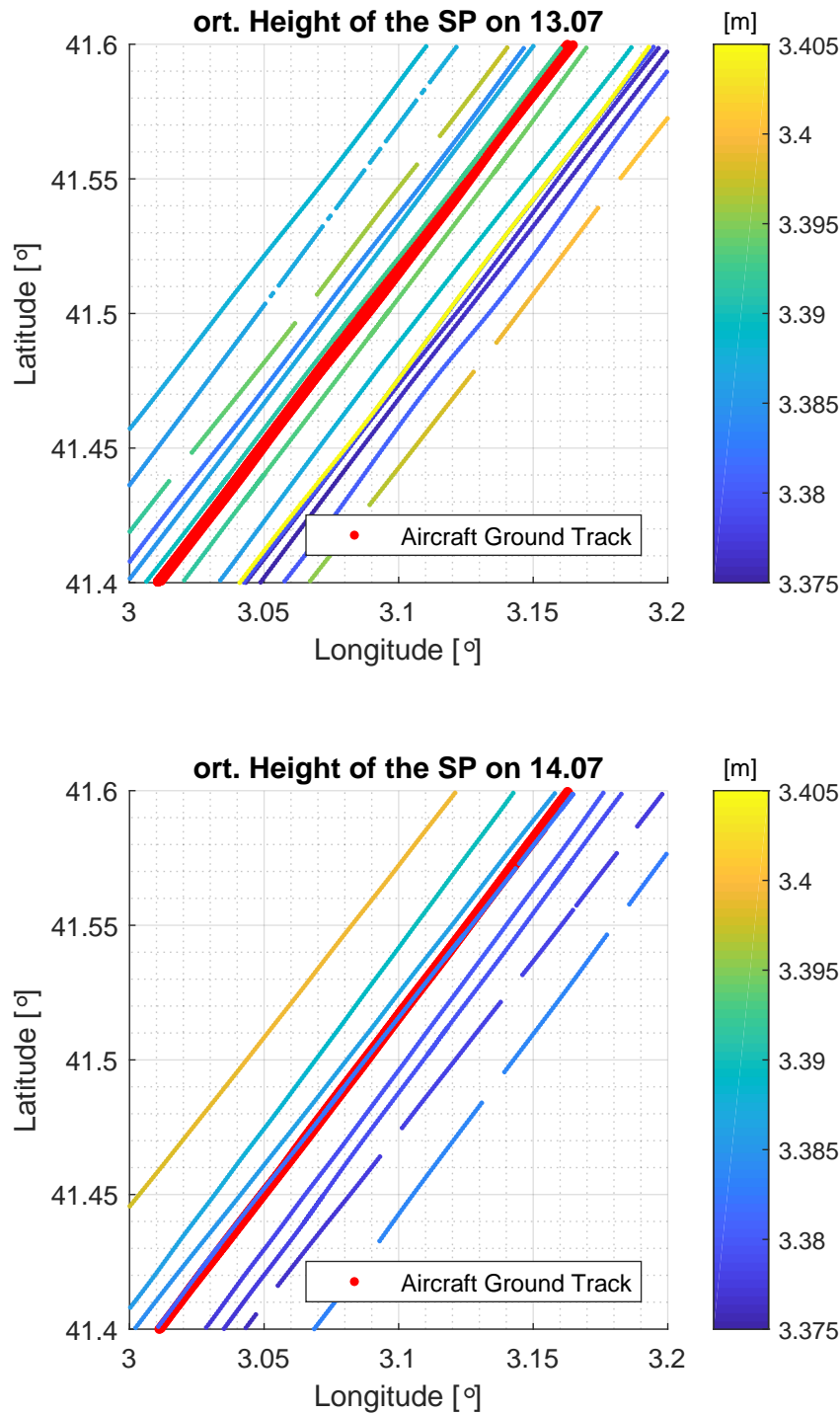


Figure 3.13: The ort. Height of the Specular Point (for a small Area)

The mean orthometric height of this area calculated on 13.07 is 3.3880 m and on 14.07 is 3.3836 m. There is only a small height difference, 4.4 mm between the two consecutive days. A more significant or even periodic change of the height is expected if more measurement on more days are dedicated.

Further more, in this figure the ground track of the aircraft is also demonstrated, plotted with red dot on the bottom. We can see that fast all specialr points distributed within 5 km on both sides of the aircraft ground track, so an area with round 10 km in cross direction could be covered in such a campaign. Obviously this result mainly depends on two variate, the elevation angle of the observation and the height of the receiver. So we could simply change the flight height to a higher level if a wider area of sea surface is of interest.

Chapter 4

Conclusion and Outlook

4.1 Conclusion

In this thesis a method to deal with the sea surface altimetry by using GNSS-Reflectometry is presented. The GNSS-R measurement delivers an important information: the delay between the direct and the reflected signal at the time they arrive at the receiver. The sea surface height is solved mainly through two iterative algorithms, the one is the comparison between the two total length path in order to know if the tentative SSH should be increased or decreased, the other one occurs on the Earth geoid/an elevated surface so that the specular point is approached. What should be paid attention to is that the measured delay consist of several small part besides the geometric delay, for example the atmosphere delay due to the troposphere and the instrument delay caused by the separately installed antennas. Each kind of these fragment should be taken into account and be precisely calculated or estimated.

After the introduction of the method a two day's campaign is applied as an example, an area about 140 km long and 10 km wide for both days was covered and the ellipsoidal-/orthometric height is estimated.

We can analyze these results in two ways. Firstly, if we just focus on one elevation map, e.g. the ell. height on 13.07 (figure 3.10, first panel). All measurements on this map was done in a short period of time and we can see the height variation from one place to another. This makes it possible to analyze if there are some unusual natural hazard like Tsunamis which could approach the coast rapidly is appearing, and if there are, a timely warning could be send out before the disaster. Secondly, we can compare two or a series of elevation map from different days, e.g. the two flight discussed in chapter 3, in order to obtain a secular change of the sea surface height.

4.2 Outlook

With more GNSS satellite constellations and advanced hardware in the future, the reflected GPS signals will soon become a more powerful source of data for scientists to get better understanding of global ocean/land surface characteristics, ocean safety, climate change and global warming. Also the new developments and applications are expected for the future space-based missions at a high temporal-spatial resolution. Furthermore, it should be free for public community and cover the entire globe as well. In addition, the bistatically reflected signals from the GNSS needs to be further extended to monitor more details of Earth's surface characteristics

in the future, such as the ocean wave and eddy, ocean salinity, internal states of sea ice, storm surge height, tsunami wave propagation and dynamics, land and flow motions, landslide and subsidence as well as geohazard warning system [12].

Bibliography

- [1] Campaigns - Test GOLD-RTR. https://www.ice.csic.es/research/gold_rtr_mining/test_gold_rtr.php.
- [2] The Campaigns and the Map. https://www.ice.csic.es/research/gold_rtr_mining/campaigns.php.
- [3] Geometry of a typical Strip-Mapping Synthetic Aperture Radar Imaging System. <http://merrbys.co.uk/about/introduction>.
- [4] GOLD-RTR MINING. https://www.ice.csic.es/research/gold_rtr_mining/index.php.
- [5] Leap Second. https://en.wikipedia.org/wiki/Leap_second.
- [6] Measurement of Earth Reflected Radio-navigation Signals by Satellite. <http://merrbys.co.uk/about/introduction>.
- [7] Orthometric Height. <https://www.spektrum.de/lexikon/geowissenschaften/orthometrische-hoehe/11712>.
- [8] Passive Reflectometry and Interferometry System. http://m.esa.int/Our_Activities/Space_Engineering_Technology/PARIS.
- [9] E. Cardellach, F. Fabra, O. Nogues Correig, S. Oliveras, S. Ribo, and A. Rius. GNSS-R Ground-based and airborne Campaigns for Ocean, Land, Ice, and Snow Techniques: Application to the GOLD-RTR Data Sets. *Radio Sci.*, 2011. doi: 10.1029/2011RS004683.
- [10] Spilker et al. Global Positioning System: Theory and Applications. *Inst. of Aeronaut. and Astronaut., Washington, D. C.*, 1996.
- [11] S. Jin, E. Cardellach, and F. Xie. *GNSS Remote Sensing*. Springer, 2014. ISBN: 978-94-007-7482-7.
- [12] S. Jin and A. Komjathy. GNSS Reflectometry and Remote Sensing: New Objectives and Results. *Advances in Space Research*, 2010.
- [13] F. Krumm. *Referenzsysteme*. Institute of Geodesy, University Stuttgart, 2013. <http://www.gis.uni-stuttgart.de/edu/study/bscgug/>.
- [14] D. McCarthy and G. Petit. IERS Conventions. *IERS Tech. Note*, 2004.
- [15] M. Neira. A passive Reflectometry and Interferometry System (PARIS): Application to Ocean Altimetry. *ESA Journal*, 1993.
- [16] A. E. Niell. Global Mapping Functions for the atmospheric Delay at Radio Wavelengths. *J. Geophys. Res.*, 1996. doi:10.1029/95JB03048.

- [17] R. N. Treuhaft, S. T. Lowe, C. Zuffada, and Y. Chao. GPS Altimetry over Crater Lake. *Geophysical Research Letters*, 2001.
- [18] K. Yu, C. Rizos, and A. Dempster. Bistatic Sensor Experiment. <http://www.garada.unsw.edu.au/reports.html>.